LIMNOLOGY and OCEANOGRAPHY

ASLO

Limnol. Oceanogr. 65, 2020, 2603–2617

doi: 10.1002/lno.11473

Life and death of *Crocosphaera* sp. in the Pacific Ocean: Fine scale predator–prey dynamics

Mathilde Dugenne,* Fernanda Henderikx Freitas, Samuel T. Wilson, David M. Karl, Angelicque E. White

Department of Oceanography, University of Hawaii at Manoa, Honolulu, Hawaii

Abstract

In the North Pacific Subtropical Gyre, the daily pulse of photosynthetic carbon (C) fixation is closely balanced by losses. This concert of growth and loss is driven by a diverse assemblage of plankton, including the diazotroph *Crocosphaera* sp. While primary production is relatively well characterized in this ecosystem, the extent of C transfer to secondary producers is poorly constrained. Here, we use automated imaging flow cytometry and population modeling to study the coupling of C production by *Crocosphaera* and subsequent grazing by nanoplanktonic protists. *Crocosphaera* cells represent on average 30% of the nanoplankton detected by the Imaging FlowCytoBot in the surface layer of mesoscale eddies during summertime. The size spectra show a maximum in the frequency of *Crocosphaera* doublet cells just prior to mitotic division at midday, with an average estimated growth rate of 0.8 ± 0.5 d^{-1}. We also identified potential predators by fitting a Lotka–Volterra model to plankton time series observations. Significant predators include the dinoflagellates *Protoperidinium* and *Dinophysis* as well as the ciliate *Strombidium*, which were all imaged with *Crocosphaera* in food vacuoles. The estimated C demand of the main grazers fluctuated between 25% and 250% of *Crocosphaera* new production in an anticyclonic eddy where we observed the onset of a *Crocosphaera*-driven bloom. Heterotrophic *Protoperidinium* drove most of the estimated C demand, with grazing rates nearly equivalent to *Crocosphaera* growth rates (0.6 ± 0.4 d^{-1} on average), but saturating at high prey concentrations. Our novel results demonstrate tight coupling between specific protistan predators and a diazotrophic prey.

Marine primary production is essential to buffer the emissions of atmospheric CO_2, to provide organic matter to marine food webs, and to drive Earth's climate. In the highly stratified North Pacific Subtropical Gyre (NPSG), the supply rate of nitrogen (N) and phosphorus (P) limit phytoplankton growth and hence rates of net primary production (Karl 2002). In these N-deplete ecosystems, the activity of N_2 fixing (diazotrophic) organisms (Carpenter and Capone 2007) can fuel new production (Karl et al. 1997) and alter the ecological stoichiometry of dissolved pools (Weber and Deutsch 2014; Letelier et al. 2019).

Depending on the season, new production based on N_2 fixation by a consortium of diazotrophs known to include *Trichodesmium*, *Richelia*, *Crocosphaera* (*UCYN-B*), *Calothrix*, *Gloeothece*, and *UCYN-A* supplies 26–47% of the production available for export in the NPSG (Böttjer et al. 2017). The relative contributions of each of these diazotrophic groups to production over time are poorly understood in the NPSG, as is the trophic fate of newly introduced diazotrophic N. Recent studies have begun to tease apart the relative production and fate of specific diazotrophs in the NPSG. For example, Wilson et al. (2017) estimated that C fixation by the autotroph *Crocosphaera* alone could account for ~ 11% of export production. These authors also reported the partitioning of the *Crocosphaera watsonii* population into two distinct size classes: a small size class with a mean cell diameter of 2.1 ± 0.5 μm and a large size class with a mean cell diameter of 5.0 ± 0.8 μm. Each size class could be represented by multiple strains (Webb et al. 2009). Using continuous underway flow cytometry, Wilson et al. (2017) revealed clear diurnal patterns in the small cell populations with light-driven growth during the day, followed by nighttime loss via respiration. Estimated growth rates (0.6 ± 0.2 d^{-1}) were closely balanced by estimated mortality due to grazing and/or viral infection (0.7 ± 0.2 d^{-1} on a single day).

While it is clear that production and loss of *Crocosphaera* are tightly coupled in the NPSG, the relative grazing pressure and the specific grazers of this important diazotroph are

*Correspondence: dugennem@hawaii.edu

Additional Supporting Information may be found in the online version of this article.

unknown. Using the classical dilution method, Calbet and Landry (1999) compared the grazing pressure exerted by different zooplankton size fractions on picophytoplankton (0.2–2.0 μm, encompassing a fraction of the small *Crocosphaera* subpopulation). They showed that the fraction of 2–20 μm grazers was responsible for most of the ingestion of *Prochlorococcus*. In this size range, there is a diverse consortium of unicellular eukaryotes (protists) that consume phytoplankton via strict heterotrophy or mixotrophy. The assemblage is generally dominated in biomass by dinoflagellates, ciliates, or rhizaria (Pasulka et al. 2013), which specifically prey on cyanobacteria (Vors et al. 1995; Hartmann et al. 2012; Deng et al. 2020). Most of the organic matter assimilated by grazers is likely remineralized since only 2–17% (5.6% on average) of the C fixed by photosynthesis is eventually exported from the euphotic layer (Karl et al. 1996). More recently, Karl et al. (2012) showed the multidecadal stability of the trophic transfer efficiency at Sta. ALOHA, with the exception of the summer export pulse putatively driven by diatom–diazotroph associations. This stability likely emerges from the strong coupling between trophic levels on a daily timescale (Viviani et al. 2011), as indicated by the diel periodicity of particulate organic carbon (POC) or the beam attenuation proxy thereof (Cullen et al. 1992; White et al. 2017). A few group- or taxa-specific studies support this statement, for instance *Prochlorococcus* (Ribalet et al. 2015), *Synechococcus* (Liu et al. 1995), *Crocosphaera* (Wilson et al. 2017) and a group of picoeukaryotes (Selph et al. 2005) all present similar daily growth and loss rates. Nonetheless, this ecosystem suffers from a lack of direct measurements or proxies for taxa-specific periodic metabolic processes (Hu et al. 2018), and more generally in microbial ecology, we know more about the factors controlling phytoplankton growth than we do for grazing (Calbet and Landry 2004).

In this article, we used high frequency image analyses and population models to specifically characterize the daily growth and grazing losses of the large cell-size subpopulation of the diazotroph *Crocosphaera*. We hypothesize that this population of *Crocosphaera* should be efficiently grazed by nanoplanktonic protists (10–20 μm) given its size, especially if its density is high enough to support predator–prey encounters (Hansen et al. 1994). Automated imaging flow cytometry, which captures the abundance of both the large size class of *Crocosphaera* as well as protistan grazers, provides a novel tool to test this hypothesis and estimate taxa-specific growth and loss rates, rarely accessible in the field.

Material and methods

Research expedition

Between 26 June 2017 and 15 July 2017, we participated in the MESO-SCOPE (Microbial Ecology of the Surface

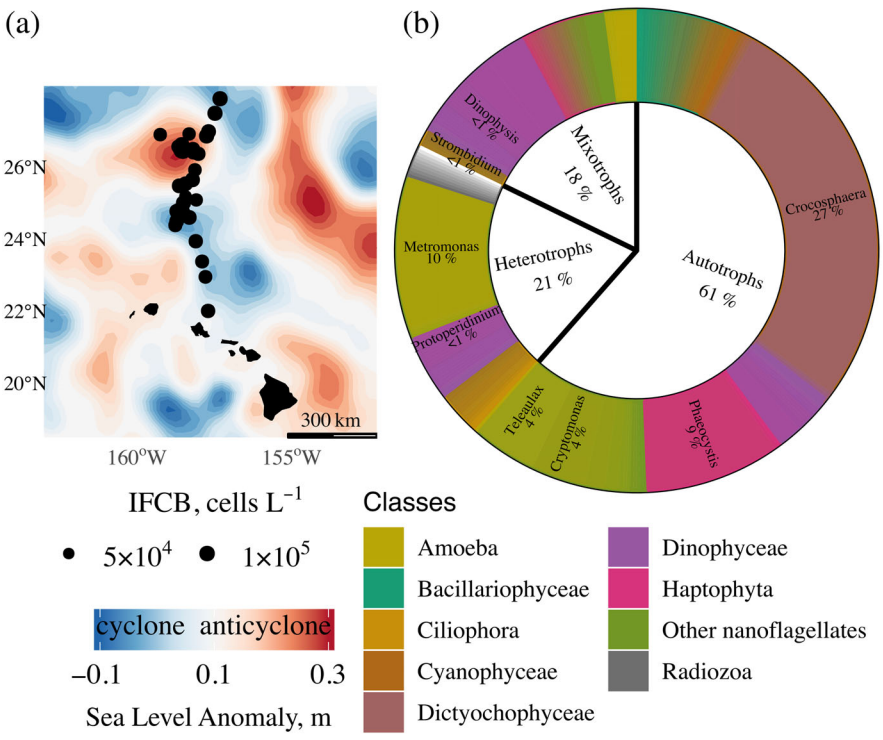

Fig. 1. Plankton enumeration during the MESO-SCOPE cruise. (**a**) Regional map of weekly mean sea surface height anomalies for 08 July 2017–14 July 2017 derived from AVISO (https://www.aviso.altimetry.fr/). The cell concentration of ~ 4–100 μm particles are shown as circles along the cruise-track. Note that the cruise crossed over anticyclonic (red) and cyclonic (blue) eddies. (**b**) Average contribution (%) of autotrophic and mixotrophic/heterotrophic phylum (assigned per literature) to the total cell concentration of observed nanoplankton (4–20 μm). Other nanoflagellates include species of cryptophytes, choanoflagellates, prasinophytes, chrysophytes, etc.

Ocean–Simons Collaboration on Ocean Processes and Ecology) cruise aboard the R/V *Kilo Moana*. The expedition targeted a specific eddy dipole located 300 km north of Oahu, Hawaii. The location of the dipole was identified using maps of sea level anomaly (https://www.aviso.altimetry.fr/) and chlorophyll a (http://marine.copernicus.eu/) measured from satellite prior to the expedition (Fig. 1a). The initial survey consisted of a N to S dipole transect from the northern edge of the anticyclonic eddy to the southern edge of the cyclonic eddy between 29 June 2017 and 02 July 2017. After the mapping phase, we followed a Lagrangian drifter (World Ocean Circulation Experiment Surface Velocity Profile; Pacific Gyre) within the cyclonic eddy between 03 July 2017 and 07 July 2017. Lastly, the Lagrangian survey in the anticyclone spanned 08 July 2017–12 July 2017. Along the cruise track, we measured sea surface temperature, incident light intensity, nutrient concentrations, and plankton abundance based on imaging flow cytometry. Mixed layer depth (MLD) was calculated as the depth where temperature differs by > 0.2°C from values at 10 m (Kara et al. 2000). Light intensity at our sampling depth (7 m) was estimated from surface measurements (LI-COR) and the coefficient of light extinction with depth, K_{PAR} (0.038 ± 0.002 m^{-1} on average), was determined from vertical profiles of a HyperPro hyperspectral radiometer (Letelier et al. 2017).

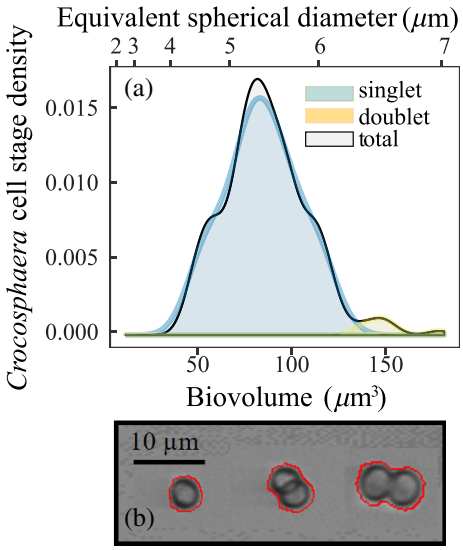

Fig. 2. The stage-specific size spectra of *Crocosphaera* cells derived from the classification of the IFCB images (*see* Supplementary Material) during the MESO-SCOPE cruise. (**a**) Singlet cells, of modal size 75 μm^3 (5.5 μm ESD), are associated with the G1/*S* phases of the cell cycle phases and doublets, 150 μm^3 (6.6 μm ESD), with G2/M. (**b**) the automated identification of singlet and doublet cells relied on the estimation of the biovolume density based on cell outlines (red lines) and was used to determine *Crocosphaera*-specific growth rates. ESD, Equivalent Spherical Diameter.

Plankton imaging and enumeration

During the MESO-SCOPE cruise, surface seawater was supplied by a magnetic centrifugal pump in continuous flow through mode from ~ 7 m depth via the ship's uncontaminated seawater system. Discrete samples were collected from Niskin® bottles at 5 m depth and analyzed within 2 h to ensure that plankton cells, especially fragile ciliates, were not underestimated in underway samples (*t*-test, $n = 12$, p-value = 0.48). High resolution (3.2 pixels per μm) images of suspended particles in the size range of ~ 4–100 μm were acquired with an Imaging FlowCytoBot (IFCB) triggering on both particle scatter and chlorophyll fluorescence to allow the individual enumeration and measurement of cell size for both phytoplankton and zooplankton. During MESO-SCOPE, autotrophic nanoplankton accounted for 63% of the total cell concentration of detectable particles in the 4–20 μm size range. In comparison, nanozooplankton, including both known heterotrophic and mixotrophic species, contributed 37% of imaged particles (Fig. 1b). *Crocosphaera* numerically dominated the nanophytoplankton, accounting for 27% of the concentration on average.

Images are currently hosted on the server http://ifcb-data.soest.hawaii.edu/ and acquisition details are a component of the image files. Volume throughput was approximately 5 mL per 20 min of analysis time. Generic biovolume distributions were estimated from two-dimensional images using a modification of the distance map algorithm described in Moberg and Sosik (2012). Biovolume was then converted to equivalent spherical diameter in order to estimate the size distribution of the individual plankton.

All retrieved particles were used to train a machine learning classifier based on morphological descriptors (Sosik and Olson 2007). A subset of the *Crocosphaera* images used to train the classifier is available as Supplementary Material. Here we used a manually annotated catalog of images collected in the NPSG between 2017 and 2018 to build a diverse training dataset. Our random forest classifier currently contains 280 distinct genera distributed over classes of Dinophyceae (69), Bacillariophyceae (66), Oligotrichea (29), Prymnesiophyceae (26), Polycystina (18), Chrysophyceae (8), Cyanophyceae (7), Acantharia (6), Dictyochophyceae (5), Oligohymenophorea (4), or Cryptophyceae (3). After the initial automated classification, the overall error rate of the algorithm scored at 22%. The error for the numerically dominant diazotroph (*Crocosphaera*) and zooplankton (*Strombidium*, *Protoperidinium*, and *Dinophysis*) detected in this study were 20%, 6%, 3%, and 9%, respectively. To improve the accuracy of planktonic diversity estimates and negate the misclassification inherent to the random forest approach, we manually annotated the output of the random forest classification with the resulting classes shown in Fig. 1b. A quantitative analysis of *nifH* transcript abundance by qPCR confirmed *Crocosphaera* was dominant during the cruise, whereas morphologically similar diazotrophs (*UCYN-C*) were not detected in either eddy feature (J. Zehr pers. comm.); this gives us

confidence in our taxonomic description of this classifier as *Crocosphaera* sp.

According to Fig. 1b, the dominant nanophytoplankter in the surface layer was *Crocosphaera* whereas several dinoflagellates and ciliates comprised the majority of mixotrophs/heterotrophs. During the Lagrangian sampling, we assume that their temporal distributions are representative of the surface layer with little entrainment by physical movements (including transient MLD variations or active vertical migration), and therefore only result from the balance between growth and loss. We detail our approach along with model parameters and assumptions inherent to the estimations of growth production and loss by predation in Supplementary Table S1.

Intrinsic growth

We estimated the number of cells formed each day by binary division, whereby a doublet cell splits into two identical singlet cells, to determine *Crocosphaera* intrinsic growth rates. Using the specific image classification, we examined the daily evolution of the cell size spectrum as singlets, typical of phase *G*1/*S*, progressively increased in size in preparation for the effective separation of doublet cells (phase *G*2/*M*) (Fig. 2). The fraction of *Crocosphaera* in *G*2/*M* phase, *f*(*G*2/*M*), at any time (*t*) can be expressed as per McDuff and Chisholm (1982) where N (cells L^{-1}) is the total number of cells observed initially (t_i) and at the end of the terminal event (t_d).

$$f(G2/M) = \frac{N(t_d)}{N(t_i)} - 1 \tag{1}$$

The duration of the terminal event, $t_d - t_i$ (d), marking effective separation of *G*2/*M* cells (Mitchinson 1971) can then be calculated as per Carpenter and Chang (1988) which is derived from a maximum of singlet cells at t_1 and a maximum of doublet cells at t_2:

$$t_d - t_i = 2(t_2 - t_1) \cdot \frac{\sum_i \log_e\left(1 + f_i(G2/M)\right)}{\sum_i \log_e\left(1 + f(G2/M) + f_i(S)\right)} \tag{2}$$

Thus, *Crocosphaera* daily growth rates (μ, d^{-1}) can be calculated by combining Eq. 1 and Eq. 2 as per Carpenter and Chang (1988) where n is the number of samples in a 24 h cycle:

$$\mu(t) = \frac{1}{n(t_d - t)} \sum_{i=1}^{n} \log_e\left(1 + f_i(G2/M)\right) \tag{3}$$

As singlet cells turn into doublets depending on the amount of C fixed via photosynthesis, we calculated the response of hourly division, $\mu(E)$ (h^{-1}), derived from hourly *f* (*G*2/*M*), to light intensity, E (μmol quanta m^{-2} s^{-1}), using the equation described in Webb et al. (1974):

$$\mu(E) = \mu_{\max} \frac{E}{E_k} \exp\left(1 - \frac{E}{E_k}\right) \tag{4}$$

Primary productivity of the imaged *Crocosphaera* population (PP, μg C L^{-1} d^{-1}) was estimated from the new biomass of cells formed by binary fission over 24 h, using the daily average growth rates ($\mu(t)$, d^{-1}) reported in Eq. 3, the daily initial cell abundance ($N(t)$, cells L^{-1}) and cellular carbon quota (Q_C, pg C $cell^{-1}$). We converted singlet cells modal biovolume to Q_C using the allometric regression intercept (0.26) and slope (0.86) reported in Menden-Deuer and Lessard (2000) for nanoplankton.

$$PP(t) = [N(t + dt) - N(t)]Q_C \times 10^{-6} \tag{5}$$

with $N(t + dt)$ depending on the daily growth rate $\mu(t)$

$$PP(t) = [\exp(\mu(t)) - 1]N(t)\left[0.26V^{0.86}\right] \times 10^{-6}$$

Loss by predation

We estimated the extent of *Crocosphaera* cell removal each day using the IFCB observations of grazer dynamics fit to a predator–prey model. The Lotka–Volterra model was used to reflect the observed temporal changes in *Crocosphaera* abundance, noted x (prey L^{-1}), as a function of daily growth rate, μ (d^{-1}), estimated in the previous section, and grazing mortality per predator, m_y ($predator^{-1}$ d^{-1}), controlled by the ingestion of a specific grazer population of density y (predators L^{-1}) (Volterra 1926).

$$\begin{aligned} \frac{dx}{dt} &= \mu x - m_y xy = (\mu - m)x \\ \frac{dx}{dt} &= \mu\left(1 - \frac{m}{\mu}\right)x \end{aligned} \tag{6}$$

with $m = m_y y$ (d^{-1}), the overall grazing rates and $\frac{m}{\mu}$, the C demand.

For a given gross growth efficiency (GGE) ε (Table S1), the grazing term promotes the growth of the predator population which decays at a constant rate, noted d (d^{-1}).

$$\frac{dy}{dt} = \varepsilon m_y xy - dy \tag{7}$$

To screen for *Crocosphaera* potential predators, we estimated the mortality rate of a given predator population, m_y ($predator^{-1}$ d^{-1}) by fitting the previous ordinary differential equation (ODE) model to its specific time series using the equivalent linear regression model.

$$\frac{dx}{dt} = \mu x - m_y xy \tag{8}$$

Or $X = \beta_x + \beta_{xy} y$ with $X \sim \frac{\Delta \log_e x}{\Delta t}$, $\beta_{xy} = -m_y$ ($predator^{-1}$ d^{-1}), $\beta_x = \mu$ (d^{-1}).

Note that we ensured m_y remained positive when fitted to grazer dynamics (Eq. 7), in order to distinguish predation from resource competition interactions. We tested the linear regression coefficients against the null hypothesis (Wald test) to identify any significant top-down control on the dynamics of *Crocosphaera* among the imaged zooplankton. In addition, a comparison of reference values and estimates of the linear regression coefficient for a set of grazing rates ranging between 4×10^{-1} and 4×10^{-5} d^{-1} is provided in Table S2. The linear regression model appears accurate over the range of grazing rates tested, yielding an average ± 15% error. To account for daily variability in plankton grazing pressure and pseudoreplication in our high frequency dataset, we developed a linear mixed-effect model corresponding to the linear regression. We estimated a unique set of coefficients for each given period (daily random effects). Part of this variability is historically explained by a set of intrinsic and extrinsic factors. The latter typically reflects density-dependent processes such as the response of predator ingestion to prey concentration (i.e., functional response), denoted m_{xy} (prey predator^{-1} d^{-1}) hereafter. When grazing rates reached saturation at high prey density, we parameterized the functional response following Eq. 9 to fit a hyperbolic Holling type II model (*nls* R function) with a prey affinity determined by the half-saturation coefficient, k_x (prey L^{-1}), and the feeding saturation rate, $m_{\max}$ (prey predator^{-1} d^{-1}) (Mullin et al. 1975). This model deviates from the general Holling functional response by assuming that only a subset of the *Crocosphaera* population, noted x_{eff} (prey L^{-1}), as opposed to the total population, can be grazed upon.

$$m_{xy}\left(\text{prey predator}^{-1}\,\text{d}^{-1}\right) = m_{\max}\left(\frac{x_{\text{eff}}}{k_x + x_{\text{eff}}}\right) \qquad (9)$$

$$x_{\text{eff}}\left(\text{prey L}^{-1}\right)\begin{cases} 0 & \text{for} \quad x < \tau \\ x - \tau & \text{for} \quad x \geq \tau \end{cases}$$

Equation 9 relates grazer ingestion rates to their prey concentration above the refuge capacity, τ (prey L^{-1}) (Table S1). The refuge capacity can also be estimated knowing grazer specific encounter rates E (L d^{-1}) and handling time h (d) (Table S1), as formulated in Eq. 10. In this model, τ (prey L^{-1}) corresponds to the concentration of prey that allows at least one encounter with the grazer, depending on the radius of the prey r (μm), directly determined in this study, and swimming speed v (μm s^{-1}) during the period equivalent to the predator handling time.

$$\tau\left(\text{prey L}^{-1}\right) = \frac{1}{Eh} = \frac{1}{\frac{3}{2}\pi r^2 v h} \qquad (10)$$

At high prey concentration, the density-dependent ingestion rates m_{xy} (prey predator^{-1} d^{-1}) scale up to the saturation maximum, $m_{\max}$. This maximum depends on the predator feeding strategy and the time it takes to handle their prey, h (d). Hence, Eq. 9 may be rewritten as:

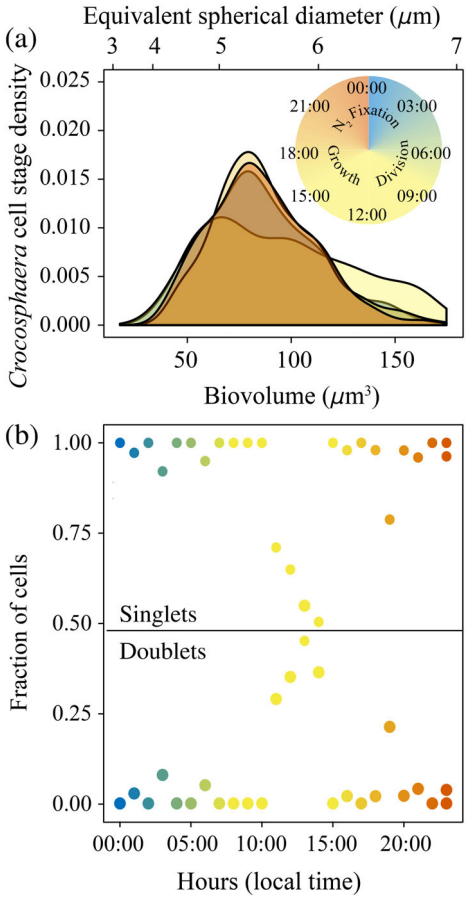

Fig. 3. (**a**) An example of the daily evolution of the *Crocosphaera* stage-specific size spectra on 12 July 2017 to illustrate the partitioning of cellular C assimilation, division and N_2 fixation. (**b**) Singlet cells assimilate C in the early morning (top panel), progressively turning into doublets (bottom panel), whose maximum fraction is usually observed at midday. After they divide, doublets are effectively separated into two singlets cells, which remain in this stage until the next morning.

$$m_{xy} = c_{\max}\left(\frac{x_{\text{eff}}}{1 + x_{\text{eff}} c_{\max} h}\right) \text{with } h = \frac{1}{m_{\max}}\,(\text{d}) \quad \text{and } c_{\max} = \frac{1}{h k_x}\left(\text{L predator L}^{-1}\,\text{d}^{-1}\right) \qquad (11)$$

Using the expression of the functional response in Eq. 9, we can rearrange the prey ODE (Rosenzweig and MacArthur 1963) into:

$$\frac{dx}{dt} = \mu x - m_{\max}\left(\frac{x_{\text{eff}}}{k_x + x_{\text{eff}}}\right) \quad y = \mu x - m_{\max} f(x) y \quad \text{with } f(x) = \frac{x_{\text{eff}}}{k_x + x_{\text{eff}}} \qquad (12)$$

Using the specific time series of plankton imaged with the IFCB, we applied a simple prey–predator model (Lotka–Volterra)

via linear regression to screen for putative interactions and estimate the C fluxes between *Crocosphaera* and its grazers via the combined estimations of growth and grazing rates (Table S1). This model can be easily expanded to any broad plankton community; however, additional techniques, such as uptake of fluorescently labeled algae (Martinez et al. 2014), will be required to validate the model fits, albeit with their own assumptions and uncertainties. We also compared daily estimation of grazing rates by a mixed-effect model to prey availability to parameterize specific functional responses.

Results

Crocosphaera growth

Using the continuous imaging of surface populations during the MESO-SCOPE cruise, we followed the daily evolution of cell growth stages for *Crocosphaera* (Fig. 3).

The singlet cells grew in size during phase *G1/S* between 06:00 and 09:00 local time (LT), in preparation for division, marking the effective separation of a doublet cell into two singlets (Fig. 3a). A fraction of the doublet cells began to divide in the early morning, around 09:00 LT, but the largest proportion of doublets was observed at midday (Fig. 3b), reflecting the increase in cell abundance during the day as cells progressed in the cell cycle. After the peak of division, cells re-entered the *G1/S* phase and subsequently began to increase in size reaching a mode of 5.5 μm (90 μm^3) around 22:00 LT. Around midnight, the size spectrum of singlet cells narrowed to a mode of 4.85 μm (60 μm^3) due to respiration, setting the stage for subsequent nighttime N_2 fixation. The evolution of the size distribution was coherent with the timing of *Crocosphaera* diel dynamics observed in laboratory cultures and in situ (Wilson et al. 2017).

Population abundance increased progressively during the photoperiod by a factor of 1.9 on average, yielding a net growth rate of 0.66 d^{-1} (Fig. 4). The average minimum concentration (~ 20,000 cells L^{-1}) was generally observed an hour before the onset of cell division (08:00 LT) and gradually increased throughout the day until dusk to ~ 40,000 cells L^{-1} (Fig. 4a). The growth response to light (Fig. 4b) indicates a population capable of achieving maximal division rates at low light levels (40 ± 13 μmol quanta m^{-2} s^{-1}), and the absence of

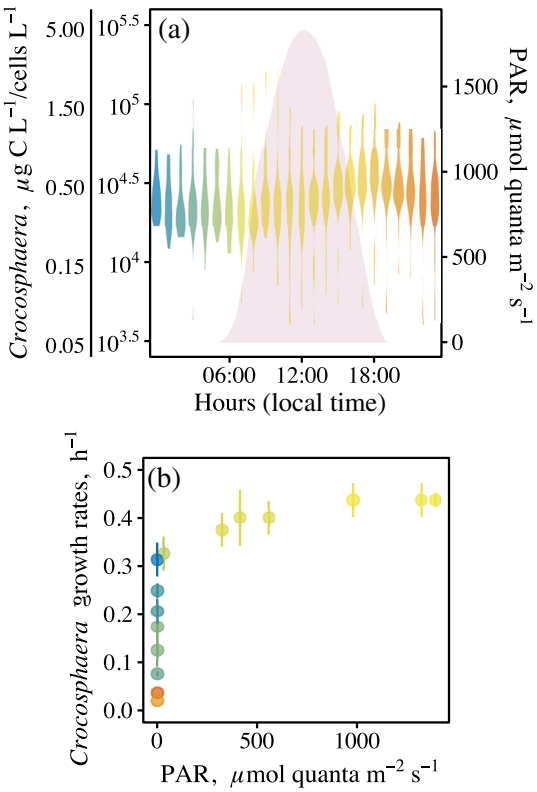

Fig. 4. (**a**) The daily abundance and carbon biomass of *Crocosphaera* during MESO-SCOPE increased under daylight as a result of intrinsic growth and declined at night due to net grazing losses. (**b**) the response of hourly division capacity, derived from hourly f(G2/M), to ambient irradiance is determined by a light optimum, E_k, of 40 μmol quanta m^{-2} s^{-1} and light-saturated growth rates of 0.4 h^{-1}. The color-code refers to the daily clock presented in Fig. 3a.

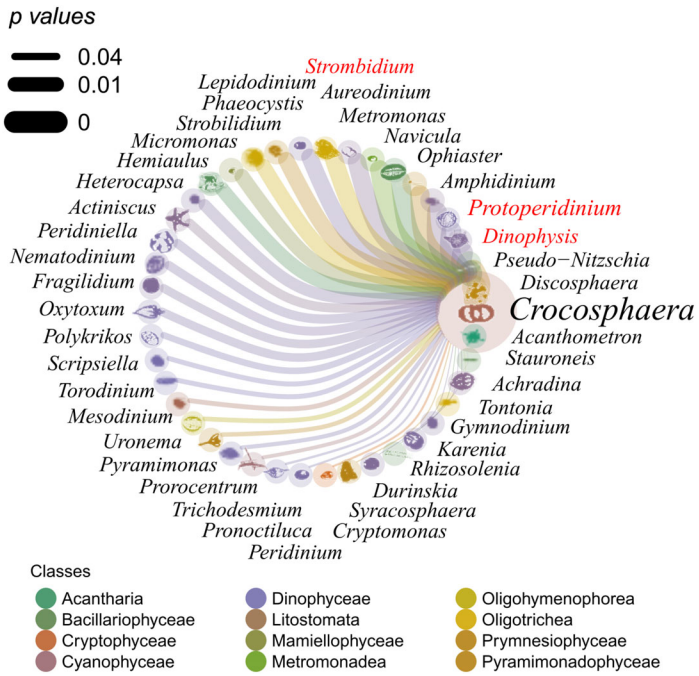

Fig. 5. Network of *Crocosphaera* potential grazers based on the fit of the prey–predator model described in Eq. 8. The *p*-values (inverse edge thickness), arranged counterclockwise, indicate evidence for a significant negative interaction with *Crocosphaera*, as between a predator and its prey. Direct evidence of grazing was provided by the IFCB images for the grazers annotated in red. The color-code is identical to the classes presented in Fig. 1b. In importance, potential grazers include numerous dinoflagellates (purple) and ciliates (yellow) of the class Oligohymenophorea and Oligotrichea.

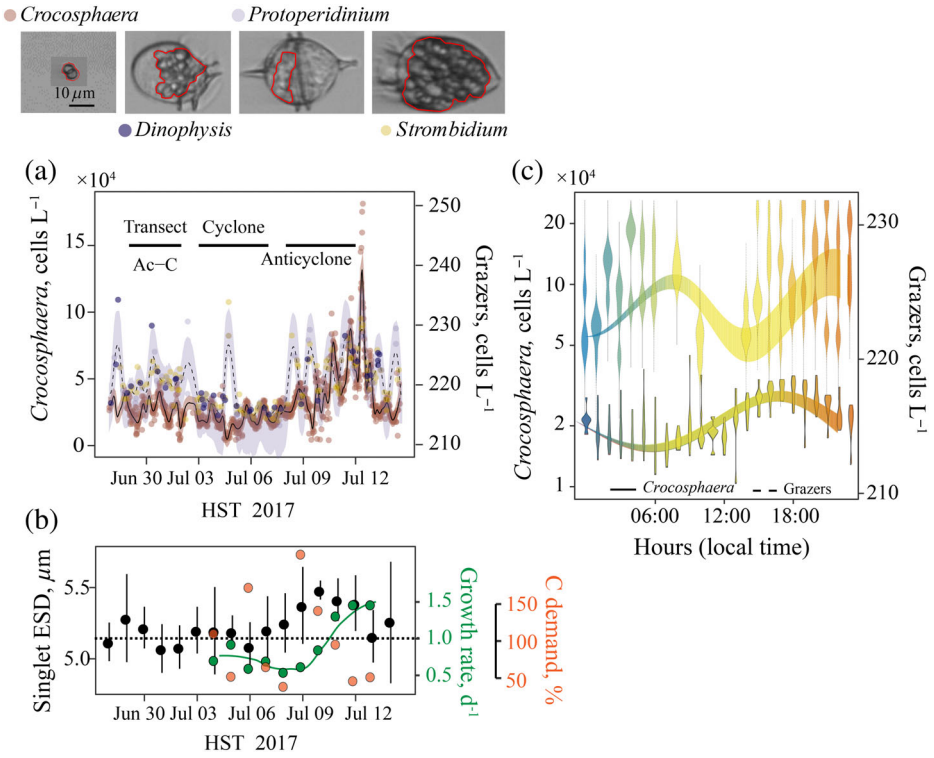

Fig. 6. (**a**) Prey–predator dynamics of *Crocosphaera* grazers, pictured ingesting *Crocosphaera* cells (outlined in red, top panel), evidenced by automated imaging during the MESO-SCOPE cruise. The upper horizontal lines mark the duration of the Lagrangian surveys in each eddy center. The lines and polygons represent the fit and 95% confidence interval of the Lotka–Volterra mixed-effect model (R^2: 0.72). (**b**) Daily average (± SD) of *Crocosphaera* growth rates, C demand, and singlet cells equivalent spherical diameter. (**c**) Hourly distributions of *Crocosphaera* and grazer abundances with the fitted Lotka–Volterra model confidence interval. The color-code refers to the daily clock presented in Fig. 3a. ESD, Equivalent Spherical Diameter.

photoinhibition within the measured PAR range, coherent with the increase of cells abundance throughout the entire photoperiod.

In contrast, net losses were restricted to nighttime and remained roughly in balance with daily production (Fig. 4a). Only within the anticyclonic eddy did *Crocosphaera* production exceed cell loss. In this mesoscale feature, the concentration of cells increased at a rate of ~ 10,000 cells L^{-1} d^{-1} to a maximum concentration of 200,000 cells L^{-1} observed on 12 July 2017.

Crocosphaera grazing

Numerous heterotrophic and mixotrophic protists coexisted with *Crocosphaera* during the MESO-SCOPE cruise (Fig. 1b). To identify potential grazers, we examined the goodness of fit of their specific dynamics to a prey–predator Lotka–Volterra model, with *Crocosphaera* as the prey (*see* Material and methods: Loss by predation). A significant coefficient assumes the predator concentration increases with a timelag after prey undergo cellular division and subsequently decrease as food becomes limited. The network of *Crocosphaera* potential grazers is presented in Fig. 5. Out of the 200 genera tested, 40 seemed to interact with *Crocosphaera*, presenting *p*-values less than 0.05. The significant interactions involved numerous genera of Dinophyceae (Myzozoa), Prymnesiophyceae (Haptophyceae), Oligotrichea (Ciliophora), Bacillariophyceae (Ochrophyta), Mamiellophyceae (Chlorophyta), and Acantharia (Radiozoa). Key grazers linked to *Crocosphaera* dynamics include specific mixotrophic coccolithophores like *Discosphaera*, ciliates such as *Strombidium*, *Uronema* or *Tontonia*, nanoflagellates (e.g., *Metromonas*), and dinoflagellates (e.g., *Protoperidinium*), all of which showed high *Crocosphaera*-specific grazing rates (based on significant fits to Eq. 8; data not shown). The network also includes autotrophic taxa, such as *Pseudo-nitzschia*, which were not grazing on *Crocosphaera* but whose dynamics are negatively correlated to *Crocosphaera* (data not shown). The dinoflagellates *Protoperidinium*, *Dinophysis*, and the ciliate *Strombidium*, included in this network were all observed appearing to have ingested *Crocosphaera* cells (Fig. 6). For these genera, we used the fit of the Lotka–Volterra model to estimate the impact of modeled specific grazing on *Crocosphaera* dynamics (Table 1).

The daily grazing rates derived from the mixed prey–predator regression varied significantly across taxa and the sampling period. Among the three predators, *Protoperidinium* induced the strongest pressure on *Crocosphaera* daily mortality with predicted rates up to 1.3 d^{-1}. Those rates often exceeded *Crocosphaera* growth rates, resulting in a variable dynamic balance. According to the model fits, *Strombidium* only exercised transient top-down control inside both eddies with rates of 0.2–0.5 d^{-1}. *Dinophysis*

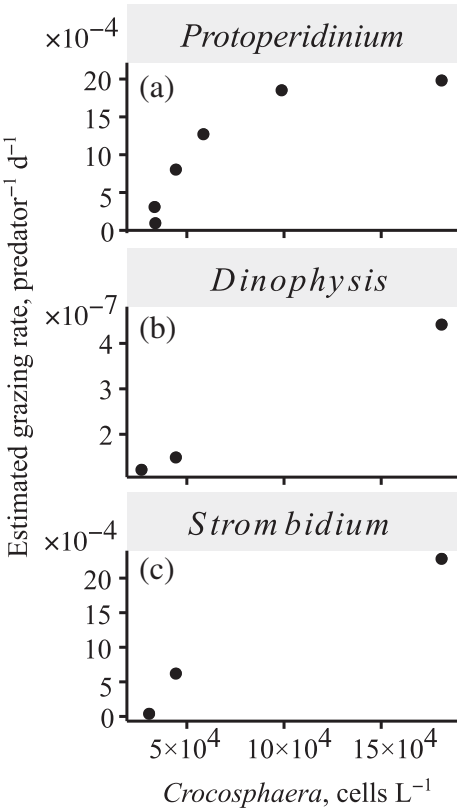

Fig. 7. The density-dependence of *Crocosphaera* mortality estimated from a Lotka–Volterra mixed-effect regression model. The per capita grazing rates of the heterotroph Protoperidinium (a) increased with prey concentration and eventually reached saturation (**a**) while saturation rates were not apparent for the mixotrophs *Dinophysis* (**b**), and Strombidium (**c**).

appeared to influence *Crocosphaera* dynamics with a significantly lower intensity, as individual daily mortality rates did not exceed 1×10^{-4} d^{-1}.

The highest estimate of mortality rates averaged 0.4 ± 0.3 d^{-1} (mean ± SD) in the cyclone and increased in the anticyclone to 0.8 ± 0.6 d^{-1} in response to enhanced *Crocosphaera* productivity. Growth rates reached on average 1.2 ± 0.5 d^{-1} in the anticyclone compared to 0.6 ± 0.2 d^{-1} within the cyclone. The estimations, based on the daily fractions of doublet cells (Eq. 1), generally exceeded the sum of mortality rates, leaving some of the *Crocosphaera* C production in excess.

During the anticyclone Lagrangian sampling, the overall estimated C demand, m^*/μ, decreased below 100%, and *Crocosphaera* abundance began to increase (Fig. 6a). During this phase, *Crocosphaera* productivity was elevated (3.1 ± 2.6 μg C L^{-1} d^{-1}) as compared to the cyclone (0.9 ± 1.1 μg C L^{-1} d^{-1}), and led to the increase of singlet cells size (Fig. 6b). As only a small fraction of newly produced cells was lost to predation, the diazotroph abundance progressively increased within the anticyclone (Fig. 6a).

Plankton coupled dynamics

Plankton abundance remained highly synchronous with the circadian clock throughout the entire sampling period, despite the day-to-day variability in estimated growth and grazing rates (Fig. 6b). Within each eddy, the MLD remained stable, and so the observed changes are presumed to be biological in origin rather than due to entrainment/dilution (Table 1). The predator/prey mixed model captured 72% of the variability of *Crocosphaera* dynamics throughout the

Table 1. Individual daily grazing rates estimated by linear mixed-effect regression for *Crocosphaera* grazers during the MESO-SCOPE Lagrangian surveys.

Hydrology	MLD (m)	Daily rates					
		Crocosphaera			*Dinophysis*	*Protoperidinium*	*Strombidium*
		PP (μg C L^{-1} d^{-1})	μ (d^{-1})	m^*/μ (%)	m (d^{-1})	m (d^{-1})	m (d^{-1})
Cyclone	—	0.32±0.13	0.6±0.2	80±70	3×10^{-5}	0.4±0.3	0.03±0.07
03 Jul 2017	—	—	0.61	109	3×10^{-5}	0.5	0.17
04 Jul 2017	40±4	0.5	0.9	33	—	0.3	—
05 Jul 2017	39±4	0.2	0.47	191	—	0.9	—
06 Jul 2017	37±3	0.4	0.6	50	—	0.3	—
07 Jul 2017	40±3	0.3	0.4	15	—	0.06	0.001
Anticyclone	—	3.2±2.4	1.2±0.5	100±90	$4\pm5\times10^{-5}$	0.8±0.6	0.1±0.2
08 Jul 2017	28±2	0.4	0.5	250	1×10^{-4}	1.2	0.04
09 Jul 2017	34±2	0.9	0.8	150	—	1.2	—
10 Jul 2017	34±5	4.0	1.4	90	—	1.3	—
11 Jul 2017	34±4	4.7	1.6	25	1×10^{-4}	0.4	—
12 Jul 2017	31±7	6.1	1.6	32	—	—	0.52

±, mean ± SD; PP, *Crocosphaera* primary productivity estimated from growth rates using Eq. 5; μ, *Crocosphaera* intrinsic growth rate derived from daily fractions of doublet cells; m, *Crocosphaera*/grazer individual mortality rate; m^*, sum of individual mortality rates.

sampling period. The dissimilarity among plankton dynamics also indicates that changes in the MLD, affecting all non-motile plankton equally, is not responsible for the observed patterns of distribution between eddies (data not shown).

Crocosphaera and its grazers displayed alternating peak times (Fig. 6c), with the peak of *Crocosphaera* cell abundance occurring around dusk (18:00 LT) and the peak of grazer cells occurring early in the morning. The decrease of *Crocosphaera* after dusk coincided with the increase in grazer abundance. The daily variations of grazer concentrations were consistent across genera. Both *Strombidium* and *Protoperidinium* followed a regular pattern marked by the progressive increase of their respective concentrations between 18:00 and 06:00 LT. *Dinophysis* appeared less synchronous to the photoperiod in general, as its concentration oscillated with a periodicity of 15 h. The overall concentration of grazers ranged between 200 and 300 cells L^{-1}. In the cyclone, the growth of *Crocosphaera* (which rarely exceeded 0.6 d^{-1}), appears to have been effectively controlled by *Strombidium*, *Protoperidinium*, and potentially other grazers not captured by our approach. The estimation of grazing demand reached 100% on the first day of the cyclonic survey and remained high over the 4 d of sampling, resulting in *Crocosphaera* steady-state dynamics (Fig. 6b).

Conversely, the unbalanced *Crocosphaera* dynamics in the anticyclone was controlled mostly by *Protoperidinium*, whose predicted grazing rates appeared strongly limited by prey availability (Fig. 7a). The concentration of *Crocosphaera* controlled the ingestion rates of *Protoperidinium*, in accordance with the functional response (Eq. 9). At high concentrations (~ 2×10^5 cells L^{-1}), grazing rates of *Protoperidinium* reached a saturation maximum which was not apparent for *Dinophysis* (Fig. 7b) or *Strombidium* (Fig. 7c). The parameterization of *Protoperidinium* grazing derived from the predator/prey model is presented in Table 2 along with *Crocosphaera*'s presumed primary grazers. The GGE, ε, fitting the Lotka–Volterra dynamics to *Crocosphaera* and grazer biomass, ranged between 20% and 44%. The highest efficiency was estimated for *Strombidium* and *Dinophysis* (30% and 44% respectively) and decreased to 20% for *Protoperidinium*. This grazer effectively consumed *Crocosphaera* when cell concentrations exceeded 30,000 cells L^{-1}, a specific refuge capacity τ linked to the availability of prey determined by the predator encounter rates and handling time. With a half-saturation constant of 23,000 cells L^{-1}, the volume of water that *Protoperidinium* needs to clear to support a biomass of 0.05 ± 0.07 μg C L^{-1} is approximately 30 μL of water $cell^{-1}$ d^{-1} (Table 2).

Simulations of *Crocosphaera* dynamics and potential bloom implications

Using the set of growth and loss parameters described in the previous sections, we predicted the fluctuations of prey and predator dynamics beyond the sampling period and as a function of grazing strategies, with (Eq. 12) or without (Eq. 6) apparent saturation of estimated grazing rates (Fig. 8a).

A ratio of predator to prey C biomass of 0.12 and 0.05 in the cyclone and anticyclone, close to the observed ratios between

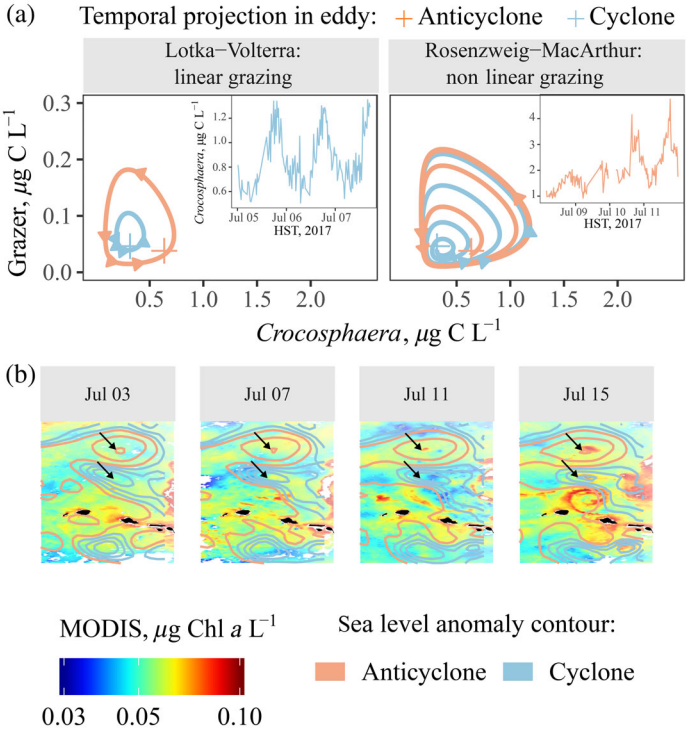

Fig. 8. (**a**) Temporal projection of *Crocosphaera* and its predator dynamics as a function of grazing strategies for the cyclone (blue) and anticyclone (red): A linear rate fits the Lotka–Volterra model (left panel) while a saturating rate is expressed in the Rosenzweig-MacArthur model (right panel). Initial conditions (crosses) corresponding to the initial biomass in each eddy are projected in time using a fixed set of parameters: μ = 1.2 d^{-1}, m/m_{max} = 0.4/0.6 d^{-1}, ε = 0.2, k_x = 0.11 μg C L^{-1}, τ = 0.15 μg C L^{-1}, d = 0.18 d^{-1}. Inserts exemplify how *Crocosphaera* concentration in the cyclone is better matched by the linear model, whereas nonlinear grazing is better able to explain the increase in *Crocosphaera* over time in the anticyclone. (**b**) The predator saturation (nonlinear grazing) significantly expands *Crocosphaera* productivity over several days, and could explain the high Chl *a* patch observed on MODIS imagery by 15 July 2017, 3 d after the end of the survey in the anticyclone. AVISO SLA contours are overlaid in B and eddy centers are indicated with arrows.

Protoperidinium, *Dinophysis*, and *Strombidium* biomass reported in Table 2, were used as initial values to determine the temporal evolution of *Crocosphaera* biomass in each eddy. Using a linear grazing rate, in the case of no apparent saturation, the biomass of predator and prey oscillate around 0.09 ± 0.04 μg C L^{-1} and 0.11 ± 0.07 μg C L^{-1}, respectively (Fig. 8a). In this model, both prey and predator biomass vary along a unique limit cycle whose amplitudes depend on both the set of parameters and the initial conditions set by the water mass.

For nonlinear grazing, with rates following a hyperbolic curve, the C flux between a prey and its predator significantly increases after several days. The saturation of predation, reflecting the estimation of *Protoperidinium* grazing rates near a prey concentration of 2×10^5 cells L^{-1} (Fig. 7a), allows prey biomass to expand over time. Also the prey refuge, 30,000 cells L^{-1} for *Crocosphaera* (Table 2), prevents the consecutive extinction of both the prey and the predator (Fig. 7a). Prey and predator should reach a stable

Table 2 Grazing parameterization estimated by linear mixed-effect regression (Eq. 8) for *Crocosphaera* grazers during the MESO-SCOPE Lagrangian surveys. For *Protoperidinium*, the parameters estimates and confidence intervals fitting the hyperbolic functional response (Eq. 9, *see* Fig. 7a) were predicted using the R function *nls*.

	Dinophysis	*Protoperidinium*	*Strombidium*
Predator : prey C	0.13*/0.07**	0.12/0.05	0.14/0.06
m (d^{-1})	$6\times10^{-4}\pm7\times10^{-4}$	0.52±0.38	0.14±0.17
ε (% C assimilation)	44±3	20±3	30±12
k_x (prey L^{-1})	—	23,000±20,00	—
τ (prey L^{-1})	—	31,600±4000	—
$\hat{\tau}$ (prey L^{-1})	—	30,010	—
c_{max} (L $cell^{-1}$ d^1)	—	3×10^{-5}	—
h (d)	—	1.4±0.2	—

$\hat{\tau}$, refuge capacity estimated via encounter rate using a swimming speed of 260 μm s^{-1} (Schuech and Menden-Deuer 2014) and prey equivalent spherical diameter of 5 μm.
*Cyclone.
**Anticyclone.

limit cycle after 5 d, with average biomass of 0.68 and 0.05 μg C L^{-1}, respectively. The simulation of *Crocosphaera* dynamics based on this model in the anticyclone effectively mirrored the observations (Fig. 6a) and could potentially explain the onset of the high chlorophyll (Chl *a*) patch appearing 3 d after the end of the sampling period (Fig. 8b). The Chl *a* concentrations of ~ 0.05 μg Chl *a* L^{-1} between 07 July 2017 and 12 July 2017, consistent with discrete shipboard measurements (0.05 ± 0.003 μg Chl *a* L^{-1}), doubled to 0.1 μg Chl *a* L^{-1} by 15 July 2017 and remained constant after that time (as observed via satellites).

Discussion

Mesoscale variability of *Crocosphaera* and associated grazers

A mesoscale transect in July 2017 recorded concentrations of 4–8 μm *Crocosphaera* (Fig. 2) as high as 2×10^5 cells L^{-1}. These cells numerically dominated the detectable stock of nanoplankton (Fig. 1) and the *nifH* transcripts abundance (J. Zehr pers. comm.) in the surface layer. Both cell size and concentration oscillated daily (Fig. 3) and the overall carbon biomass of this diazotroph ranged between 0.15 and 1.0 μg C L^{-1} (Fig. 4). In the NPSG, *Crocosphaera* biomass generally peaks in July, September, and October (Pasulka et al. 2013). The late summer peak, close to 0.5 μg C L^{-1}, contrasts with the low wintertime standing stock, which does not exceed 0.2 μg C L^{-1} (Pasulka et al. 2013). *Crocosphaera* regularly blooms in this ecosystem due to its ability to fix N_2 and its capacity for enhanced growth rates. Using the population-specific size spectra, we were able to measure *Crocosphaera* daily growth rates and the subsequent grazing rates consistent with the daytime production of cells and nighttime losses. There was considerable variability between the two mesoscale structures (Table 1). In the cyclone, growth rates averaged 0.6 ± 0.2 d^{-1}, an estimate close to the values reported in Wilson et al. (2017). In contrast, the average growth rates in the anticyclone reached 1.2 ± 0.5 d^{-1} and coincided with a reduction in estimated grazing rates (Table 1). These growth rates are similar to estimates by Turk-Kubo et al. (2018) at 45 m of 1.6 ± 0.5 d^{-1} for the diazotrophs UCYN-B(= *Crocosphaera*), UCYN-A, UCYN-C, and *Richelia*. Consequently *Crocosphaera* productivity, 1.94 ± 2.31 μg C L^{-1} d^{-1} for the entire study (Table 1), likely accounted for a large fraction of total oxygen-based gross primary production, which peaked at 14 ± 1.5 μg C L^{-1} d^{-1} in the anticyclonic eddy (S. Ferrón pers. comm.). Assuming *Crocosphaera* respires between 15% and 25% of its daily gross primary production (Inomura et al. 2019), this suggests that the nitrogen fixer can sporadically support net primary production rates equivalent to the contribution of picoeukaryotes (1.58 ± 0.75 μg C L^{-1} d^{-1}) or *Prochlorococcus* (1.12 ± 0.52 μg C L^{-1} d^{-1}), previously measured at 5 m depth in the NPSG (Rii et al. 2016).

While the bulk grazing rates of microzooplankton on phytoplankton in the NPSG historically ranges between 0.18 and 0.45 d^{-1} (Schmoker et al. 2013), we predicted rates as high as 1.3 d^{-1} using a Lotka–Volterra regression model. In this ecosystem, we know that the abundance of the heterotrophic community is both maximal at the surface and during summertime, reflecting the abundance of small prey like *Crocosphaera* (Pasulka et al. 2013). During the MESO-SCOPE cruise, the abundance of the main secondary producers (i.e., ciliates and dinoflagellates) estimated with the IFCB averaged 500 ± 1000 cells L^{-1}, in agreement with previous quantifications based on traditional microscopy in the NPSG (Selph et al. 2005; Girault et al. 2016). The potential grazers of *Crocosphaera* shown in Fig. 5 represent a large diversity of secondary producers, dominated by genera of dinoflagellates and ciliates known to graze on the numerically dominant cyanobacteria genera, *Prochlorococcus* and *Synechococcus* in the NPSG (Frias-Lopez et al. 2009), and representatives recently confirmed to also feed on *Crocosphaera* in culture (Deng et al. 2020). These grazers include numerous prymnesiophytes, nanoflagellates like *Metromonas*, ciliates like *Uronema* or *Strobilidium*, and dinoflagellates like

Gymnodinium. The negative interaction identified between *Crocosphaera* and *Pseudo-nitzschia* in the network could have been mediated by copper rather than predation, which specifically increases the former productivity (Lopez et al. 2019) but inhibit the growth of *Pseudo-nitzschia* and promotes the production of the domoic acid toxin (Maldonado et al. 2002) at the concentrations measured during MESO-SCOPE (N. Hawco pers. comm.). Based on the literature, we found that most of the dinoflagellate present during the MESO-SCOPE cruise comprised mixotroph species while most of the ciliates were heterotrophs (Fig. 1b). Their variable feeding strategies have an impact on growth requirement and grazing rates (Raven 1997). The heterotroph *Protoperidinium*, for instance, shows a reduced growth efficiency GGE (ε), with 20% of their prey C incorporated into its biomass (Sailley and Buitenhuis 2014), including *Crocosphaera* (Table 2), compared to the mixotrophs *Strombidium*, and *Dinophysis*, whose GGE reach 30% and 44%, respectively (Table 2).

Relative balance of *Crocosphaera* production and grazing losses

During MESO-SCOPE, *Crocosphaera* dynamics revealed diurnal patterns of growth and strong coupling between production and loss. The nighttime losses were generally consistent with the predators dynamics; however, additional losses by viral lysis, as suggested by Hewson et al. (2009), or autolysis could have scaled up to 25% of *Crocosphaera* daily growth rates (Table S3). The abundance of *Crocosphaera* consumers followed a diurnal phasing, with a peak at dawn, following the peak of *Crocosphaera* concentration at dusk (Fig. 6). However, the balance between *Crocosphaera*-predicted growth and loss varied strongly from day to day (Table 1), which is consistent with the balance of primary production and loss via community respiration over short time scales (Ferrón et al. 2015). Across all marine ecosystems, the average C demand of secondary consumers reaches 67% of phytoplankton production and increases to 75% in subtropical ecosystems, consequently leaving excess C available for potential export or other pathways (e.g., viral lysis) (Calbet and Landry 2004). The modeled pressure exerted by *Crocosphaera* predators in the present study reached 94% ± 80% on average and even exceeded the growth capacity of the diazotroph on multiple occasions (Fig. 6b). A modification of Eq. 8 to allow additional daily constant loss rates yielded similar estimates of C demand, 86% ± 74% on average (Table S3). This control induced a strong coupling dynamics (Fig. 6) and an efficient C transfer along the foodweb. Despite the prediction of a high C demand in the anticyclone, *Crocosphaera* productivity left more C in excess (1.2 μg C L^{-1}) compared to the cyclone (0.1 μg C L^{-1}) in response to the high photosynthetic C assimilation rates associated with the increase of singlet cells size (Fig. 6b).

The coupling of planktonic population dynamics leads to several emergent properties, such as the scaling of prey–predator size and biomass (Acevedo-Trejos et al. 2015), and may even persist over climatological timescales (Hunter-Cevera et al. 2016). Since the summertime stratification of the NPSG surface layer promotes small primary producers, the optimal size of the grazers is predicted to be 3–30 μm (Vors et al. 1995). The size of *Crocosphaera* grazers encompassed the ranges 7–30 μm for *Strombidium*, 6–30 μm for *Dinophysis* and 8–25 μm for *Protoperidinium* (data not shown). The size spectra of *Crocosphaera* grazers agrees with the observations of Hansen et al. (1994) who reported ciliates as 8 times larger than their prey; flagellates, only 3 times bigger, and dinoflagellates, overlapping in size with their prey. In the case of heterotrophic dinoflagellates, the overlap with prey size and high clearance rates allow to compensate for their low GGE, in addition to increasing clearance rates. For instance, *Protoperidinium* was reported to clear up to 24 μL $cell^{-1}$ d^{-1} (Jeong et al. 2010), similar to the 30 μL $cell^{-1}$ d^{-1} we estimated in this study. With a biovolume of 1200 ± 700 μm^3, the volume of water it has to clear daily therefore corresponds to 10^7 its own body size, an effort mainly compensated by the efficiency of cruise feeding strategy (Kiorboe 2011) or diel vertical migration (Schuech and Menden-Deuer 2014).

The size spectra of *Crocosphaera* grazers ultimately controlled the respective biomass of secondary producers, varying between 0.01–0.3 μg C L^{-1}, 0.006–0.3 μg C L^{-1}, and 0.01–0.8 μg C L^{-1} for *Strombidium*, *Dinophysis* and *Protoperidinium*, respectively. Similar to considerations of size, the ratio of predator to prey biomass is well constrained and averaged 0.12, 0.14, and 0.09 for the respective genera. Using the parameterization of *Crocosphaera* grazing derived from the Lotka–Volterra model fits (Tables 1 and 2), we showed that simulated biomass should remain close to the initial ratio, even under the constraints of a density-dependent grazing pressure (Fig. 8). The simulations reproduced the periodic oscillations of phytoplankton and zooplankton biomass with a periodicity close to 24 h and bounds of 0.2–1.2 μg C L^{-1} and 0.01–0.21 μg C L^{-1}, respectively. The lower and upper bounds of *Crocosphaera* biomass are determined by a positive equilibrium, which eventually determines the biomass of *Protoperidinium*, or any other grazer (Gonzalez-Olivares and Ramos-Jiliberto 2003).

Controls of *Crocosphaera* net production in the NPSG

Diazotrophs such as *Crocosphaera* have a natural advantage in oligotrophic ecosystems as they can avoid N limitation. As a consequence, their growth rates appear to be independent of the low concentrations of inorganic N or bioavailable dissolved organic N (Zehr et al. 2017; Turk-Kubo et al. 2018), similarly to that of the nondiazotrophic cyanobacteria, *Prochlorococcus* and *Synechococcus*, whose small size and high nutrient-specific uptake affinities allow for maximum growth rates ranging from 0.4 to 1.0 d^{-1} at Sta. ALOHA (Liu et al. 1995; Vaulot et al. 1995; Ribalet et al. 2015; Berthelot et al. 2019). In this study, the daily growth rates of the large subpopulation of *Crocosphaera* (1.4–1.6 d^{-1}, Table 1) exceeded the known ranges for *Prochlorococcus* and *Synechococcus* between 10 July 2017 and 12 July 2017. *Crocosphaera* division rates were primarily controlled by light intensity, as

reported by Grimaud et al. (2014), with our data indicating a relatively low light half-saturation coefficient (40 μmol quanta m^{-2} s^{-1}, Fig. 4). The fraction of doublets thus rapidly increased at low light intensity and peaked at the maximum of daylight intensity of 500 μmol quanta m^{-2} s^{-1} observed around noon time (Fig. 4). The near-instantaneous response of cell division to light utilization results from the orchestration of daylight net growth and nighttime respiration in order to support N_2 fixation, also described for other diazotrophs like *Cyanothece* (Taniuchi et al. 2012). The daily evolution of *Crocosphaera* cell size distribution presented in Fig. 3 agrees with the preliminary field study of Wilson et al. (2017) which showed that *nifH* transcription peaks at midday, and that the metabolic utilization of respiratory C peaks around midnight to optimize the fixation of N_2 before dawn. The concurrent intensification of grazing at nighttime also reduces the likelihood of strong cell stage-specific removal, which may introduce a 20% bias in the estimate of intrinsic growth rates by the cell cycle method (Chang and Dam 1993).

The main secondary producers in this study comprised both mixotrophs which grazed on *Crocosphaera* at moderate rates (Fig. 7b,c) and heterotrophs like *Protoperidinium*, for which growth appears primarily mediated by *Crocosphaera* grazing with predicted rates saturating at high prey concentrations observed in this study (Fig. 7a). Consequently, the activity of *Protoperidinium* estimated from modeling changed with both the quantity of prey (functional response) and its own carrying capacity, reflecting the strength of intraspecific competition (logistic growth). The control of ingestion rate as a function of *Crocosphaera* concentration forces the predator to grow rapidly whenever prey are present above a given threshold and conversely decline when they become too scarce (Holling 1973). The refuge capacity reinforces the stability of the coexistence by preventing the extinction of the prey. For *Crocosphaera*, the prediction of the refuge capacity derived from the Lotka–Volterra regression was close to an independent estimation of a minimum concentration which can be encountered and handled by *Protoperidinium* within a day. Modeled predator satiation, observed for *Crocosphaera* concentration higher than ~ 1×10^5 cells L^{-1}, limits cells removal and generally results in higher C flux between the prey and the predator (Fig. 8). The appearance of a high chlorophyll patch in the anticyclone 3 d after our in situ sampling period is consistent with nonlinear grazing, as a strategy promoting *Crocosphaera* enhanced production. With an increase of 0.05 μg Chl *a* L^{-1} and a Chl *a* : C ratio of 34 (Jacq et al. 2014), the production of *Crocosphaera*, 1.4 μg C L^{-1}, could have effectively driven this satellite-observed bloom.

Conclusion

The unicellular diazotroph *Crocosphaera* appears to be able to achieve growth rates up to 1.6 d^{-1} in the NPSG, constituting a prime target for phytoplankton consumers. *Crocosphaera* likely supported a diverse assemblage of protists, mainly dinoflagellates and ciliates, constrained by the predator to prey size spectra. Estimated grazing rates varied as a complex interaction between intrinsic and extrinsic forcings; however, predator abundances responded predictably, as per Lotka–Volterra model predictions, to the increase of *Crocosphaera* cells observed during the photoperiod. The species specifically imaged grazing on *Crocosphaera* encompassed both mixotrophs (e.g., *Dinophysis* and *Strombidium*), converting new production into secondary production with a GGE of 30%, and the heterotroph *Protoperidinium* showing a reduced C conversion capacity. As a consequence of density-dependent grazing rates, C fluxes between *Crocosphaera* and its predators were higher inside an anticyclonic eddy compared to an adjacent cyclonic eddy. The results reveal a diverse community of secondary consumers, with a range of trophic strategies, as potential grazers of the diazotroph *Crocosphaera* and ultimately as controls of gross N_2 fixation in the NPSG. Along with nutrient fertilization, grazers are essential to control the fate of primary production and C fluxes in mesoscale eddies. This study also represents a novel and incubation-independent exploration of the diversity and activity of grazers of an ecologically and biogeochemically important genera, the diazotroph *Crocosphaera*, that can be expanded to other genera and other ecosystems to improve our understanding of the interplay between bottom-up and top-down controls of ocean production and microbial diversity.

References

Acevedo-Trejos, E., G. Brandt, J. Bruggeman, and A. Merico. 2015. Mechanisms shaping size structure and functional diversity of phytoplankton communities in the ocean. Sci. Rep. **5**: 1–8. doi:10.1038/srep08918

Berthelot, H., S. Duhamel, S. L'Helguen, J.-F. Maguer, S. Wang, I. Cetnič, and N. Cassar. 2019. NanoSIMS single cell analyses reveal the contrasting nitrogen sources for small phytoplankton. ISME J. **13**: 651–662. doi:10.1038/s41396-018-0285-8

Böttjer, D., J. E. Dore, D. M. Karl, R. M. Letelier, C. Mahaffey, S. T. Wilson, J. Zehr, and M. J. Church. 2017. Temporal variability of nitrogen fixation and particulate nitrogen export at station ALOHA. Limnol. Oceanogr. **62**: 200–216. doi:10.1002/lno.10386

Calbet, A., and M. R. Landry. 1999. Mesozooplankton influences on the microbial food web: Direct and indirect trophic interactions in the oligotrophic open-ocean. Limnol. Oceanogr. **44**: 1370–1380. doi:10.4319/lo.1999.44.6.1370

Calbet, A., and M. R. Landry. 2004. Phytoplankton growth, microzooplankton grazing, and carbon cycling in marine systems. Limnol. Oceanogr. **49**: 51–57. doi:10.4319/lo.2004.49.1.0051

Carpenter, E. J., and J. Chang. 1988. Species-specific phytoplankton growth rates via diel DNA synthesis. I. Concept of the method. Mar. Ecol. Prog. Ser. **42**: 105–111.

Carpenter, E. J., and D. G. Capone. 2007. Nitrogen fixation in the marine environment, p. 141–198. *In* D. G. Capone, D. A. Bronk, M. R. Mulholland, and E. J. Carpenter [eds.], Nitrogen in the marine environment. Elsevier.

Chang, J., and H. G. Dam. 1993. The influence of grazing on the estimation of phytoplankton growth rates via cell cycle analysis: Modeling and experimental evidence. Limnol. Oceanogr. **38**: 202–212. doi:10.4319/lo.1993.38.1.0202

Cullen, J. J., M. R. Lewis, C. O. Davis, and R. T. Barber. 1992. Photosynthetic characteristics and estimated growth rates indicate grazing is the proximate control of primary production in the equatorial Pacific. J. Geophys. Res. **97**: 639–654. doi:10.1029/91JC01320

Deng, L., S. Cheung, and H. Liu. 2020. Protistal grazers increase grazing on unicellular cyanobacteria diazotroph at night. Front. Mar. Sci. **7**: 1–9. doi:10.3389/fmars.2020.00135

Ferrón, S., S. T. Wilson, S. Martinez-Garcia, P. D. Quay, and D. M. Karl. 2015. Metabolic balance in the mixed layer of the oligotrophic North Pacific Ocean from diel changes in O_2/Ar saturation ratios. Geophys. Res. Lett. **42**: 1–10. doi:10.1002/2015GL063555

Frias-Lopez, J., A. Thompson, J. Waldbaeur, and S. W. Chisholm. 2009. Use of stable isotope-labelled cells to identify active grazers of picocyanobacteria in ocean surface waters. Environ. Microbiol. **11**: 512–525. doi:10.1111/j.1462-2920.2008.01793.x

Girault, M., G. Grégori, A. Barani, and H. Arakawa. 2016. A study of microphytoplankton and cyanobacteria consortia in four oligotrophic regimes in the western part of the North Pacific Subtropical Gyre and in the warm pool. J. Plankton Res. **38**: 1317–1333. doi:10.1093/plankt/fbw056

Gonzalez-Olivares, E., and R. Ramos-Jiliberto. 2003. Dynamic consequences of prey refuges in a simple model system: More prey, fewer predators and enhanced stability. Ecol. Model. **166**: 135–146. doi:10.1016/S0304-3800(03)00131-5

Grimaud, G. M., S. Rabouille, A. Dron, A. Sciandra, and O. Bernard. 2014. Modelling the dynamics of carbon–nitrogen metabolism in the unicellular diazotrophic cyanobacterium *Crocosphaera watsonii* WH8501, under variable light regimes. Ecol. Model. **291**: 121–133. doi:10.1016/j.ecolmodel.2014.07.016

Hansen, B., P. K. Bjornsen, and P. J. Hansen. 1994. The size ratio between planktonic predators and their prey. Limnol. Oceanogr. **39**: 395–403. doi:10.4319/lo.1994.39.2.0395

Hartmann, M., C. Grob, G. A. Tarran, A. P. Martin, P. H. Burkill, D. J. Scanlan, and M. V. Zubkov. 2012. Mixotrophic basis of Atlantic oligotrophic ecosystems. Proc. Natl. Acad. Sci. USA **109**: 5756–5760. doi:10.1073/pnas.1118179109

Hewson, I., et al. 2009. *In situ* transcriptomic analysis of the globally important keystone N_2-fixing taxon *Crocosphaera watsonii*. ISME J. **3**: 618–631. doi:10.1038/ismej.2009.8

Holling, C. S. 1973. Resilience and stability of ecological systems. Ann. Rev. Ecol. Syst. **4**: 1–23. doi:10.1146/annurev.es.04.110173.000245

Hu, S. K., P. E. Connell, L. Y. Mesrop, and D. A. Caron. 2018. A hard day's night: Diel shifts in microbial eukaryotic activity in the North Pacific Subtropical Gyre. Front. Mar. Sci. **5**: 1–17. doi:10.3389/fmars.2018.00351

Hunter-Cevera, K., M. G. Neubert, R. J. Olson, A. R. Solow, A. Shalapyonok, and H. M. Sosik. 2016. Physiological and ecological drivers of early spring blooms of a coastal phytoplankter. Science **354**: 326–329. doi:10.1126/science.aaf8536

Inomura, K., and others. 2019. Quantifying oxygen management and temperature and light dependencies of nitrogen fixation by *Crocosphaera watsonii*. mSphere **4**: e00531-19. doi:10.1128/mSphere.00531-19

Jacq, V., C. Ridame, S. L'Helguen, F. Kaczmar, and A. Saliot. 2014. Response of the unicellular diazotrophic cyanobacterium *Crocosphaera watsonii* to iron limitation. PLoS One **9**: 1–9. doi:10.1371/journal.pone.0086749

Jeong, H. J., Y. D. Yoo, J. S. Kim, K. A. Seong, N. S. Kang, and T. H. Kim. 2010. Growth, feeding and ecological roles of the mixotrophic and heterotrophic dinoflagellates in marine planktonic food webs. Ocean Sci. J. **45**: 65–91. doi:10.1007/s12601-010-0007-2

Kara, A. B., P. A. Rochford, and H. E. Hurlburt. 2000. An optimal definition for ocean mixed layer depth. J. Geophys. Res.: Oceans **105**: 16803–16821. doi:10.1029/2000JC900072

Karl, D. M. 2002. Nutrient dynamics in the deep blue sea. Trends Microbiol. **10**: 410–418. doi:10.1016/s0966-842x(02)02430-7

Karl, D. M., J. R. Christian, J. E. Dore, D. V. Hebel, R. M. Letelier, L. M. Tupas, and C. D. Winn. 1996. Seasonal and interannual variability in primary production and particle flux at station ALOHA. Deep-Sea Res. II **43**: 539–568. doi:10.1016/0967-0645(96)00002-1

Karl, D. M., R. Letelier, L. Tupas, J. Dore, J. Christian, and D. Hebel. 1997. The role of nitrogen fixation biogeochemical cycling in the subtropical North Pacific Ocean. Nature **388**: 533–538. doi:10.1038/41474

Karl, D. M., M. J. Church, J. E. Dore, R. M. Letelier, and C. Mahaffey. 2012. Predictable and efficient carbon sequestration in the North Pacific Ocean supported by symbiotic nitrogen fixation. Proc. Natl. Acad. Sci. USA **109**: 1842–1849. doi:10.1073/pnas.1120312109

Kiorboe, T. 2011. How zooplankton feed: Mechanisms, traits and trade-offs. Biol. Rev. **86**: 311–339. doi:10.1111/j.1469-185X.2010.00148.x

Letelier, R. M., A. E. White, R. R. Bidigare, B. Barone, M. J. Church, and D. M. Karl. 2017. Light absorption by phytoplankton in the North Pacific Subtropical Gyre. Limnol. Oceanogr. **62**: 1526–1540. doi:10.1002/lno.10515

Letelier, R. M., K. M. Björkman, M. J. Church, D. S. Hamilton, N. M. Mahowald, R. A. Scanza, N. Schneider, A. E. White, and D. M. Karl. 2019. Climate-driven oscillation of

phosphorus and iron limitation in the North Pacific Subtropical Gyre. Proc. Natl. Acad. Sci. USA **116**: 12720–12728. doi:10.1073/pnas.1900789116

Liu, H., L. Campbell, and M. R. Landry. 1995. Growth and mortality rates of *Prochlorococcus* and *Synechococcus* measured with a selective inhibitor technique. Mar. Ecol. Prog. Ser. **116**: 277–287.

Lopez, J. S., L. Lee, and K. R. M. Mackey. 2019. The toxicity of copper to *Crocosphaera watsonii* and other marine phytoplankton: A systematic review. Frontiers **5**: 1–13. doi:10.3389/fmars.2018.00511

Luo, Y.-W., et al. 2012. Database of diazotrophs in global ocean: Abundance, biomass and nitrogen fixation rates. Earth Syst. Sci. Data **4**: 47–73. doi:10.5194/essd-4-47-2012

Maldonado, M. T., M. P. Hughes, and E. L. Rue. 2002. The effect of Fe and Cu on growth and domoic acid production by *Pseduo-Nitzschia multiseries* and *Pseudo-Nitzschia australis*. Limnol. Oceanogr. **47**: 515–526. doi:10.4319/lo.2002.47.2.0515

Martinez, R. A., S. Isari, and A. Calbet. 2014. Use of live, fluorescently-labeled algae for measuring microzooplankton grazing in natural communities. J. Exp. Mar. Biol. Ecol. **457**: 59–70. doi:10.1016/j.jembe.2014.03.007

McDuff, R. E., and S. W. Chisholm. 1982. The calculation of in situ growth rates of phytoplankton populations from fractions of cells undergoing mitosis: A clarification. Limnol. Oceanogr. **27**: 783–788. doi:10.4319/lo.1982.27.4.0783

Menden-Deuer, S., and E. J. Lessard. 2000. Carbon to volume relationships for dinoflagellates, diatoms, and other protist plankton. Limnol. Oceanogr. **45**: 569–579. doi:10.4319/lo.2000.45.3.0569

Mitchinson, J. M. 1971. The biology of the cell cycle. Cambridge Univ. Press.

Moberg, E. A., and H. M. Sosik. 2012. Distance maps to estimate cell volume from two-dimensional plankton images. Limnol. Ocranogr.: Methods **10**: 276–288. doi:10.4319/lom.2012.10.278

Mullin, M. M., E. Fuglister Stewart, and F. J. Fuglister. 1975. Ingestion by planktonic grazers as a function of concentration of food. Limnol. Oceanogr. **20**: 259–262. doi:10.4319/lo.1975.20.2.0259

Pasulka, A. L., M. R. Landry, D. A. A. Taniguchi, A. G. Taylor, and M. J. Church. 2013. Temporal dynamics of phytoplankton and heterotrophic protists at station ALOHA. Deep-Sea Res. II **93**: 44–57. doi:10.1016/j.dsr2.2013.01.007

Raven, J. A. 1997. Phagotrophy in phototrophs. Limnol. Oceanogr. **42**: 198–205. doi:10.4319/lo.1997.42.1.0198

Ribalet, F., J. Swalwell, S. Clayton, V. Jimènez, S. Sudek, Y. Lin, Z. Johnson, A. Z. Worden, and E. V. Armbrust. 2015. Light-driven synchrony of *Prochlorococcus* growth and mortality in the subtropical Pacific Gyre. Proc. Natl. Acad. Sci. USA **112**: 8008–8012. doi:10.1073/pnas.1424279112

Rii, Y. M., D. M. Karl, and M. J. Church. 2016. Temporal and vertical variability in picophytoplankton primary productivity in the North Pacific Subtropical Gyre. Mar. Ecol. Prog. Ser. **562**: 1–18. doi:10.3354/meps11954

Rosenzweig, M. L., and R. H. MacArthur. 1963. Graphical representation and stability conditions of predator-prey interactions. Am. Nat. **97**: 209–223. doi:10.1086/282272

Sailley, S. F., and E. T. Buitenhuis. 2014. Microzooplankton functional responses in the lab and in the field. Earth Syst. Sci. Data Discuss. **7**: 149–167. doi:10.5194/essdd-7-149-2014

Schmoker, C., S. Hernandez-Leon, and A. Calbet. 2013. Microzooplankton grazing in the oceans: Impacts, data variability, knowledge gaps and future directions. J. Plankton Res. **35**: 691–706. doi:10.1093/plankt/fbt023

Schuech, R., and S. Menden-Deuer. 2014. Going ballistic in the plankton: Anisotropic swimming behavior of marine protists. Limnol. Oceanogr.: Fluids and Environments **4**: 1–16. doi:10.1215/21573689-2647998

Selph, K. E., J. Shacat, and M. R. Landry. 2005. Microbial community composition and growth rates in the NW Pacific during spring 2002. Geochem. Geophys. Geosyst. **6**: 1–20. doi:10.1029/2005GC000983

Sosik, H. M., and R. J. Olson. 2007. Automated taxonomic classification of phytoplankton sampled with imaging-in-flow cytometry. Limnol. Oceanogr.: Methods **5**: 204–216. doi:10.4319/lom.2007.5.204

Taniuchi, Y., Y.-L. Chen, H.-Y. Chen, M.-L. Tsai, and K. Ohki. 2012. Isolation and characterization of the unicellular diazotrophic cyanobacterium group C TW3 from the tropical western Pacific Ocean. Environ. Microbiol. **14**: 641–654. doi:10.1111/j.1462-2920.2011.02606.x

Turk-Kubo, K. A., P. Connell, D. Caron, M. E. Hogan, H. M. Farnelid, and J. P. Zehr. 2018. In situ diazotroph population under different resource ratios in the North Pacific Subtropical Gyre. Frontiers Microbiol. **9**: 1–18. doi:10.3389/fmicb.2018.01616

Vaulot, D., D. Marie, R. J. Olson, and S. W. Chisholm. 1995. Growth of *Prochlorococcus*, a photosynthetic prokaryote, in the equatorial Pacific Ocean. Science **268**: 1480–1482. doi:10.1126/science.268.5216.1480

Viviani, D. A., K. M. Björkman, D. M. Karl, and M. J. Church. 2011. Plankton metabolism in surface waters of the tropical and subtropical Pacific Ocean. Aquat. Microb. Ecol. **62**: 1–12. doi:10.3354/ame01451

Volterra, V. 1926. Fluctuations in the abundance of a species considered mathematically. Nature **118**: 558–560. doi:10.1038/118558a0

Vors, N., K. R. Buck, F. P. Chavez, W. Eikrem, L. E. Hansen, J. B. Ostergaard, and H. A. Thomsen. 1995. Nanoplankton of the equatorial Pacific with emphasis on the heterotrophic protists. Deep-Sea Res. II **42**: 585–602. doi:10.1016/0967-0645(95)00018-L

Webb, W. L., M. Newton, and D. Starr. 1974. Carbon dioxide exchange of *Alnus rubra* a mathematical model. Ecologia **17**: 281–291. doi:10.1007/BF00345747

Webb, A. W., I. M. Ehrenreich, S. L. Brown, F. W. Valois, and J. B. Waterbury. 2009. Phenotypic and genotypic characterization of multiple strains of the diazotrophic cyanobacterium *Crocosphaera watsonii*, isolated from the open ocean. Environ. Microbiol. **11**: 338–348. doi:10.1111/j.1462-2920.2008.01771.x

Weber, T., and C. Deutsch. 2014. Local versus basin-scale limitation of marine nitrogen fixation. Proc. Natl. Acad. Sci. USA **111**: 8741–8746. doi:10.1073/pnas.1317193111

White, A. E., B. Barone, R. M. Letelier, and D. M. Karl. 2017. Productivity diagnosed from the diel cycle of particulate carbon in the North Pacific Subtropical Gyre. Geophys. Res. Lett. **44**: 3752–3760. doi:10.1002/2016GL071607

Wilson, S. T., and others. 2017. Coordinated regulation of growth, activity and transcription in natural populations of the unicellular nitrogen-fixing cyanobacterium *Crocosphaera*. Nat. Microbiol. **2**: 1–9. doi:10.1038/nmicrobiol.2017.118

Zehr, J. P., J. S. Weitz, and I. Joint. 2017. How microbes survive in the open ocean. Science **357**: 646–647. doi:10.1126/science.aan5764

Acknowledgments

We thank Katie Watkins-Brandt for substantial technical contributions, Benedetto Barone for numerous comments on the manuscript and the captain and crew members of the R/V *Kilo Moana*. This work was funded by the Simons Foundation support of SCOPE (Simons Collaboration on Ocean Processes and Ecology, Award 329104 to A.E.W. and D.M.K.).

Conflict of Interest

None declared.

Submitted 29 July 2019
Revised 30 March 2020
Accepted 29 April 2020

Associate editor: Ilana Berman-Frank